Available online at www.eccomasproceedia.org
Eccomas Proceedia COMPDYN (2023) 971-981

ECCOMAS
Proceedia

COMPDYN 2023
9th ECCOMAS Thematic Conference on
Computational Methods in Structural Dynamics and Earthquake Engineering
M. Papadrakakis, M. Fragiadakis (eds.)
Athens, Greece, 12-14 June 2023

EXPERIMENT AND SIMULATION OF Q–Δ RESONANCE USING FOUR-LAYER BENDING-SHEAR TYPE SPECIMEN

Ryohei Kai[1] **and Masayuki Kohiyama**[2]

[1] School of Science for Open and Environmental Systems, Graduate School of Science and Technology, Keio University
3-14-1 Hiyoshi, Kohoku-ku, Yokohama, 223-8522, Japan
ryohei_kai@keio.jp

[2] Department of System Design Engineering, Faculty of Science and Technology, Keio University
3-14-1 Hiyoshi, Kohoku-ku, Yokohama, 223-8522, Japan
kohiyama@sd.keio.ac.jp

Abstract

Torsional vibration of buildings subjected to earthquake motion has been studied for many years, but the torsional vibration of high-rise buildings has not yet been clarified. Many previous studies have focused on eccentricity, the mismatch between the center of gravity and the rigid center, as the cause of torsional vibration. However, in buildings with no eccentricity, torsional vibrations could be observed. The authors' research group focused on the "Q–Δ effect," a phenomenon in which torsional torque is generated due to geometric nonlinearity and "Q–Δ resonance," a phenomenon in which resonance occurs when the period of torsional torque generation coincides with the natural period of the torsional mode. In order to analyze the characteristics of Q–Δ resonance, a small-scale specimen was designed and fabricated from an 81-story high-rise building with biaxially symmetrical plans, which was reduced to four stories. As a result, the torsional response of the experimental and simulation results generally agreed, confirming that the torsional response increases when the Q–Δ resonance condition is satisfied. In addition, a comparison of the torsional response with a specimen with a smaller tower ratio and less bending deformation was conducted, and it was confirmed that the peak of the torsional response was steeper in the present study case.

Keywords: Bending-Shear Type Building, Shaking Table Experiment, Torsional Response, Geometric Nonlinearity, Q–Δ Resonance, Finite Element Analysis.

ISSN:2623-3347
Peer-review under responsibility of the organizing committee of COMPDYN 2023.
doi: 10.7712/120123.10450.21152

1 INTRODUCTION

When long-period and long-duration seismic motions are generated by a large-scale earthquake, resonance phenomena could occur in high-rise buildings with long natural periods, causing the buildings to respond significantly. In fact, during the Great East Japan Earthquake, a resonance phenomenon occurred at the Sakishima government office building in Osaka Prefecture, located approximately 800 km from the epicenter, and the maximum displacement near the top floor reached 137 cm [1]. Given the imminent threat of a large-scale Nankai Trough earthquake, further research is needed on the response of high-rise buildings under long-period and long-time seismic motion input.

Although torsional vibration of buildings subjected to earthquake motion has been studied for many years, torsional vibration of high-rise buildings has not yet been clarified. Many previous studies have focused on eccentricity, the misalignment between the center of gravity and rigid center, as the cause of torsional vibration. However, it has been confirmed that torsional vibration occurs even in buildings without eccentricity. The authors' research group [2] focuses on the "*Q–Δ* effect," a phenomenon in which torsional torque is generated owing to geometric nonlinearities, and studies the "*Q–Δ* resonance," a phenomenon in which resonance occurs when the period of torsional torque generation coincides with the natural period of the torsional mode. Mizutori and Kohiyama [3] confirmed the occurrence of *Q–Δ* resonance by shaking table experiments using a one-story specimen. Anamizu and Kohiyama [4] proposed an equation of motion that considers the *Q–Δ* effect for a two-story uneccentric structure, and theoretically derived the *Q–Δ* resonance condition that considers up to the second modes of each direction mode. Shaking table experiments using a two-story specimen confirmed that torsional vibration is excited even when the *Q–Δ* resonance condition for the second mode of torsion is satisfied. Anamizu [5] derived the equation of motion for a multistory uneccentric structure considering the *Q–Δ* effect, and confirmed that *Q–Δ* resonance occurs at the natural frequency of the torsional mode predicted by shaking table experiments using a four-layer specimen. In the previous studies described above, only shear-type buildings, which do not cause bending deformation of the entire building, were considered. In this study, *Q–Δ* resonance of a flexural shear-type building with a large height/width aspect ratio and predominant flexural deformation is analyzed by shaking table experiments using a four-layer specimen. In addition, a finite element analysis of the four-layer specimen is performed to validate the shaking table experiments.

2 DESIGN AND FABRICATION OF A SMALL-SCALE SPECIMEN

2.1 Setup of super high-rise building model

To evaluate the torsional response of a flexural shear-type building, a small-scale specimen of a super high-rise building with a large height/width aspect ratio is fabricated and shaking table tests are conducted. This chapter describes the design and fabrication of the small-scale specimen. In designing the small-scale specimen, a building model is first set up as the assumed super high-rise building. The building is assumed to have a steel structure and its use is assumed to be an office. Considering that some buildings currently under construction in Japan exceed 300 m in height, the building model is assumed to have 81 stories with a story height of 4 m, the eave height being 324 m. The plan is 80 × 64 m, and the load per unit area for mass calculation in the dynamic analysis is 9,020 N/m^2 . As in Reference [5], the *Q–Δ* resonance condition is assumed to be satisfied where the sum of f_{1x} and f_{1y}, the first natural frequencies in the *x*- and *y*-directions, matches $f_{2\theta}$, the second natural frequency in the torsional direction. The first natural frequencies in the *x*- and *y*-directions are set with reference to the natural frequencies of

real buildings [6]. Here, the x-axis is taken in the direction of the strong axis, which has a shorter natural period than in its perpendicular direction. **Table 1** summarizes the natural frequencies and natural periods of the building model. **Figure 1** compares the first natural periods ratio T_{1x}/T_{1y} (= f_{1y}/f_{1x}) and the proximity to the Q–Δ resonance condition ($f_{2\theta}/(f_{1x} + f_{1y})$) between the building model and real buildings (green: the building model, blue: real buildings).

Mode	Natural frequency [Hz]	Natural period [s]
1st mode in the x-direction	0.267	3.75
1st mode in the y-direction	0.200	5.00
2nd mode in the torsional direction	0.467	2.14

Table 1: Natural frequencies and natural periods of the building models.

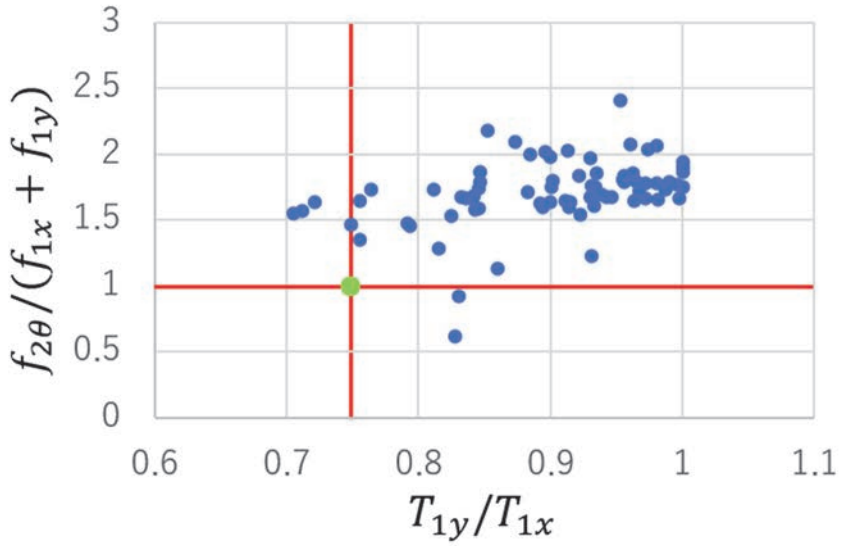

Figure 1: Comparison of natural frequency characteristic values between the building model and real buildings.

2.2 Design and fabrication of small-scale specimen

Considering the payload of shaking table and safety during the experiment, the specimen to be fabricated is a small-scale four-layer model of the building model, which is reduced according to the similarity rule. First, multiple stories in the building model are grouped into four layers, and the method of condensing each story group to a single mass is as follows. the position of the representative masses in the height direction after condensation (hereinafter referred to as "representative masses position") shall be the position satisfying the following three conditions:

I. The number of representative masses is four.
II. The number of stories in each story group is the same.
III. The representative masses are located at the middle height of each story group.

The positions of the representative masses are shown in gray in **Figure 2**. The representative mass location for the yellow layer group is 72 m above ground level. Similarly, the representative mass locations for the blue, green, and orange groups are 144, 216, and 288 m above ground level, respectively. In other words, each slab position of the small-scale specimen is designed to correspond to the 18th, 36th, 54th, and 72nd floor slab positions of the building model. The scaling factor with respect to a length is set to λ = 1/200 based on the references [4, 7]. The

target design values for the building model and the small-scale specimen are shown in **Table 2**. **Figures 3** and **4** respectively shows an overall and elevation views of the small-scale specimen fabricated based on the design target values shown in **Table 2**. **Table 3** shows the dimensions, materials, mass, and quantity of the main components of the specimen. Four fixed weights are installed on the underside of each slab. By moving the movable weights, the moment of inertia around the vertical axis passing through the center of each slab can be changed, and the design allows the first natural period in the torsional direction to be set in 12 different ways. Since the position of the fixed weight is not moved, the position of the movable weight is referred to as the "weight position" in this paper. The weight positions are named from P1 to P12 in order of placement pattern, beginning with the one closest to the center of each slab; the second natural period in the torsional direction is the shortest at P1, and longest at P12. **Figure 5(a)** and **5(b)** shows the positions of movable weights at P1 and P12.

Feature	Unit	Building model	Small-scale specimen (design target value)	Scaling factor
Plan	m	80.0 × 64.0	0.500 × 0.320	1/200
Height	m	288	1.44	1/200
Mass	kg	4.00×10^8	50.0	$1/200^3$
First natural period in the x-direction	s	3.60	0.255	$1/200^{1/2}$
First natural period in the y-direction	s	4.80	0.339	$1/200^{1/2}$
First natural period in the θ-direction	s	2.14	0.152	$1/200^{1/2}$

Table 2: Design target values for small-scale specimen.

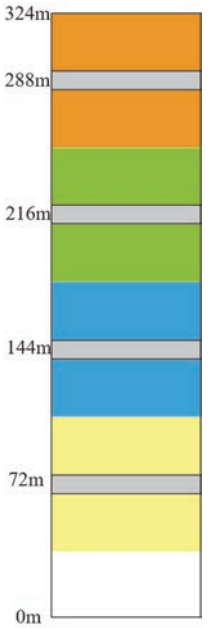

Figure 2: Location of representative masses.

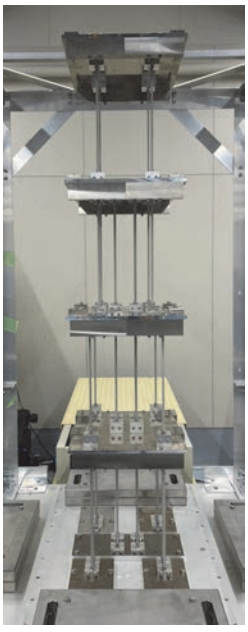

Figure 3: Overall view.

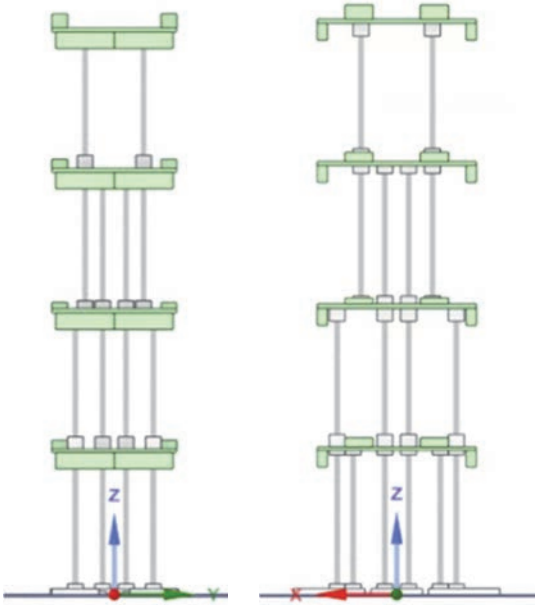

Figure 4: Elevations.

Component	Size [mm]	Material	Mass [kg]	Quantity
1st slabs	400 × 320 × 8	A5052	2.68	1
2nd, 3rd, and 4th slabs	400 × 320 × 10	A5052	3.34	3
Columns	8 × 6 × 349	YH75	0.0476	32
Fixed weights	25 × 150 × 42	SUS303	1.22	16
1st and 3rd layer weights	70 × 40 × 23	SUS303	0.497	8
2nd layer weights	70 × 40 × 15	SUS303	0.325	4
4st layer weights	70 × 40 × 36	SUS303	0.779	4
1st layer connections	19 × 40 × 12	A5052	0.020	48
2nd layer connections	19 × 40 × 32	A5052	0.058	32
3rd layer connections	19 × 40 × 20	A5052	0.035	32
4th layer connections	19 × 40 × 33	A5052	0.060	16

Table 3: The size, material, mass and quantity of main components of specimen.

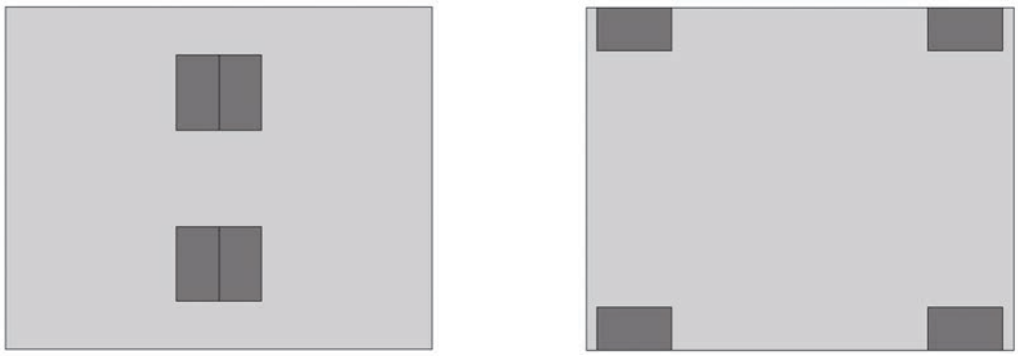

(a) P1 (b) P12

Figure 5: The position of movable weights

Eight triaxial acceleration sensors are installed, one at each of the two diagonal corners (points A and B) of the four corners of each layer slab. The translational absolute accelerations $\ddot{x}, \ddot{y}$ and rotational angular accelerations $\ddot{\theta}_z$ at the center of each slab are calculated as follows: $\ddot{x}_\mathrm{A}, \ddot{y}_\mathrm{A}, \ddot{x}_\mathrm{B}$, and $\ddot{y}_\mathrm{B}$ are the measured values of the acceleration sensors in the x- and y-directions at the points A and B of each slab, respectively. Let r_x be the distance from the x-axis to the sensor and r_y be the distance from the y-axis to the sensor, then the relationship between $\ddot{x}_\mathrm{A}, \ddot{y}_\mathrm{A}, \ddot{x}_\mathrm{B}, \ddot{y}_\mathrm{B}$ and $\ddot{x}, \ddot{y}, \ddot{\theta}_z$ is expressed as follows:

$$\begin{Bmatrix} \ddot{x}_A \\ \ddot{y}_A \\ \ddot{x}_B \\ \ddot{y}_B \end{Bmatrix} = \begin{bmatrix} 1 & 0 & -r_y \\ 0 & 1 & r_x \\ 1 & 0 & r_y \\ 0 & 1 & -r_x \end{bmatrix} \begin{Bmatrix} \ddot{x} \\ \ddot{y} \\ \ddot{\theta}_z \end{Bmatrix} \tag{1}$$

Using the least-squares method, $\ddot{x}, \ddot{y}$, and $\ddot{\theta}_z$ are obtained by

$$\begin{Bmatrix} \ddot{x} \\ \ddot{y} \\ \ddot{\theta}_z \end{Bmatrix} = \begin{bmatrix} 1 & 0 & -r_y \\ 0 & 1 & r_x \\ 1 & 0 & r_y \\ 0 & 1 & -r_x \end{bmatrix}^+ \begin{Bmatrix} \ddot{x}_A \\ \ddot{y}_A \\ \ddot{x}_B \\ \ddot{y}_B \end{Bmatrix} = \frac{1}{2} \begin{bmatrix} 1 & 0 & 1 & 0 \\ 0 & 1 & 0 & 1 \\ -\frac{r_y}{r^2} & \frac{r_x}{r^2} & \frac{r_y}{r^2} & -\frac{r_x}{r^2} \end{bmatrix} \begin{Bmatrix} \ddot{x}_A \\ \ddot{y}_A \\ \ddot{x}_B \\ \ddot{y}_B \end{Bmatrix} \tag{2}$$

where $[\ ]^+$ is the inverse of Moore-Penrose, r_x = 0.200 m, r_y = 0.160 m, and $r = \sqrt{r_x^2 + r_y^2}$.

3 SHAKING TABLE EXPERIMENTS USING A SMALL-SCALE SPECIMEN

3.1 System Identification Experiments on a Small-Scale Specimen

(1) Experimental method

To identify the dynamic characteristics of the small-scale specimen, shaking table tests were conducted using a horizontally-biaxial shaking table, San-Esu SPT2D-10K-85L-10T. First, one-directional excitation was performed in the *x*- and *y*-directions, respectively. The mass of each layer does not change even if the weights are set at positions other than P1, and thus the natural frequency and damping factor in the *x*- and *y*-directions were assumed to remain unchanged at positions P5, P7, P8, P9, P10, P11, and P12. The measured acceleration response was filtered by a 6th-order Butterworth low-pass filter with a cutoff frequency of 50 Hz. The acceleration response was then extracted for 18 s and the Ordinary MOESP method [8, 9] was used to identify the natural frequencies and mode shapes of the first to fourth modes in each direction. The excitation was conducted twice in each direction, and the average of the two values was used as the identification result.

(2) Experimental results

Table 4 shows the natural frequencies identified by the experiments. **Figures 6 and 7** show the mode shapes in the translational and torsional directions at the position P1, respectively, which are normalized so that the fourth layer displacement is 1. If we focus on the sum or difference of the natural frequencies of the modes in the translational direction in **Table 4(a)**, we can see that

$$f_{1x} + f_{1y} = 6.75 \text{ Hz} \quad (3)$$

$$f_{2x} - f_{1y} = 6.96 \text{ Hz} \quad (4)$$

The resonance condition $f_{1x} + f_{1y} = f_{2\theta}$ in equation (3) is almost satisfied at the position P10, and positions P5 and P7 are closest to the resonance condition $f_{2x} - f_{1y} = f_{2\theta}$ in equation (4), the torsional response being expected to increase at P5, P7 and P10.

Mode	Natural frequency [Hz]
f_{1x}	3.85
f_{2x}	9.86
f_{3x}	15.6
f_{4x}	21.0
f_{1y}	2.90
f_{2y}	7.48
f_{3y}	11.8
f_{4y}	15.8

(a) Translational direction

Weight position	Natural frequencies [Hz]			
	$f_{1\theta z}$	$f_{2\theta z}$	$f_{3\theta z}$	$f_{4\theta z}$
P1	2.86	7.28	10.8	15.3
P3	2.79	7.13	10.5	15.1
P5	2.73	7.00	10.3	14.8
P7	2.69	6.92	10.2	14.7
P8	2.67	6.87	10.1	14.6
P9	2.64	6.81	10.0	14.5
P10	2.61	6.74	9.95	14.4
P11	2.57	6.67	9.83	14.2
P12	2.53	6.60	9.73	14.1

(b) Torsional direction

Table 4: Natural frequencies of small-scale specimen.

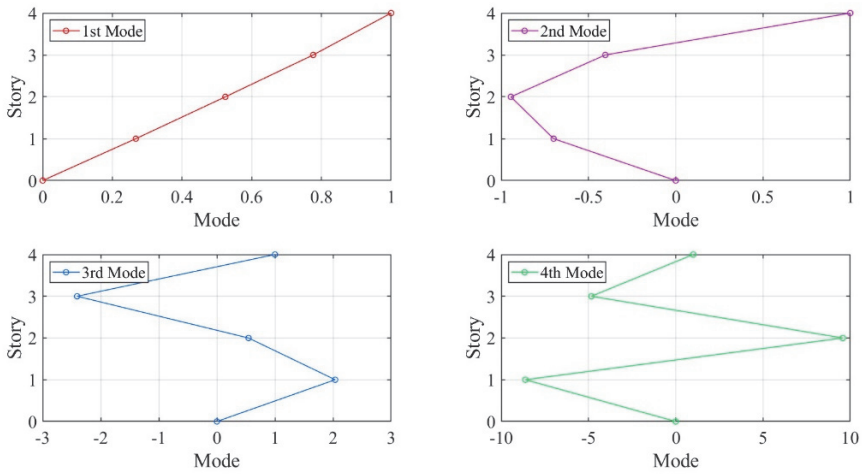

(a) *x*-direction

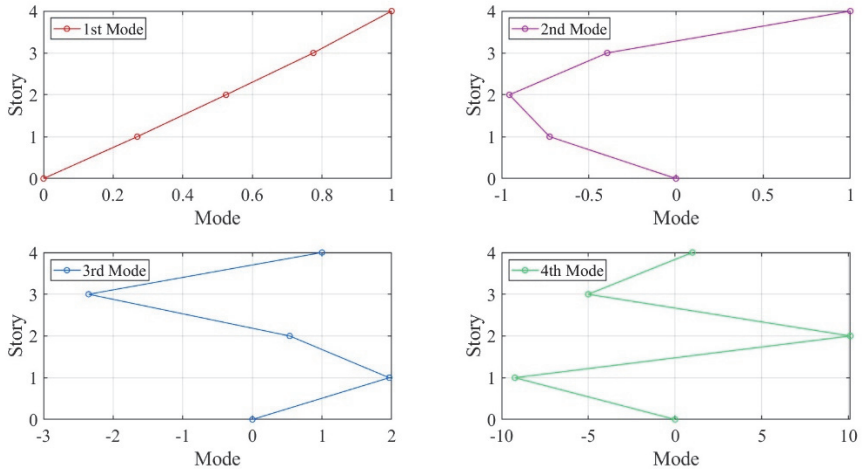

(b) *y*-direction

Figure 6: Translational mode shapes.

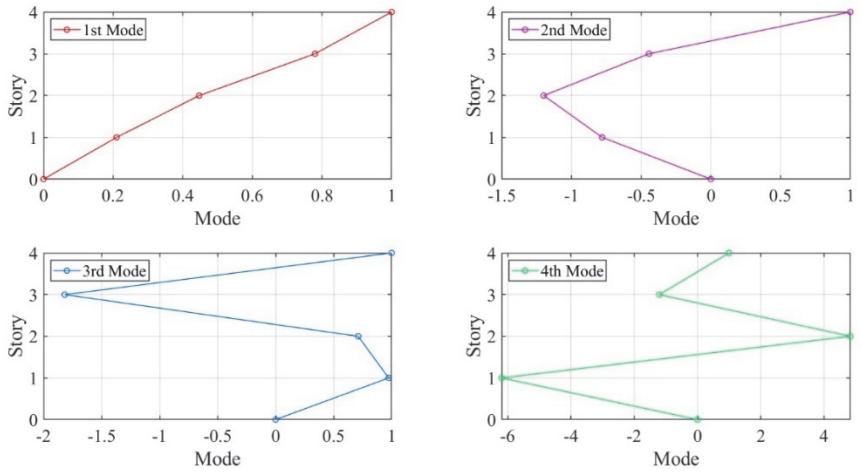

Figure 7: Torsional mode shapes.

3.2 *Q–Δ* Resonance Verification Experiment

(1) Experimental method

In this experiment, the shaking table was used to excite in two horizontal directions by two types of input motions to verify the torsional response of the small-scale specimen owing to *Q–Δ* resonance. The first input motion was sinusoidal wave shown in **Figure 8**. The second input motion was a simulated earthquake motion show in **Figure 9**, which was the measured absolute acceleration at the position P11. This input motion was a long-period seismic motion OS1 [10] for design purpose developed by the Ministry of Land, Infrastructure, Transport and Tourism, which was scaled by a factor of $1/200^{1/2}$ according to the similarity law shown in **Table 2**, and processed by a third-order Butterworth bandpass filter with a passband of 0.5–8.0 Hz.

First, the weight position was set to P1 and the specimen was excited one time each with a sinusoidal wave and simulated earthquake motion, in that order. Next, the weight was moved to position P3 and the specimen was excited in the same manner. The same procedure was repeated with the weight positions at P5, P7, P8, P9, P10, P11, and P12, in that order. The measured acceleration response was processed by a third-order Butterworth bandpass filter with a passband of 1.0–30 Hz.

(2) Experimental results

Figure 10(a) and **10(b)** shows the maximum angular acceleration at the center of gravity of the slab when subjected to the sinusoidal wave and simulated earthquake motion excitations, respectively. **Figure 10(b)** shows that the maximum angular acceleration peaks at the weight positions P8 and P11. The reason why the peak did not appear at P5, P7, or P10, which was expected, is discussed below.

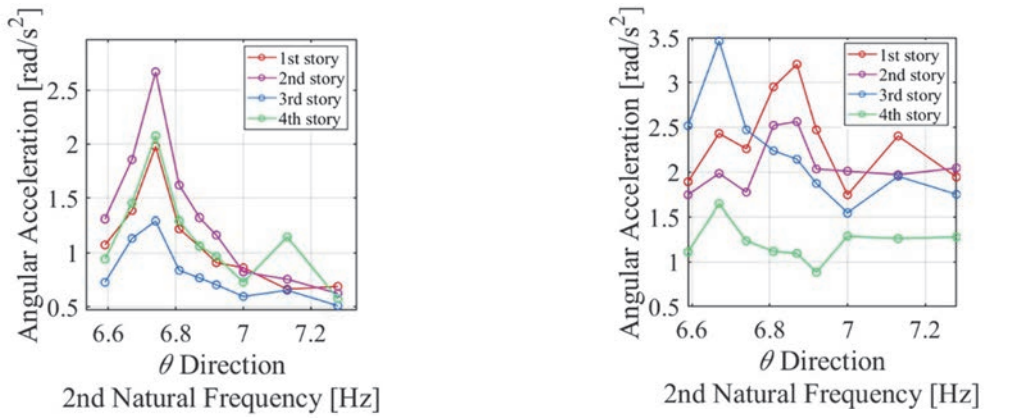

(a) Sinusoidal wave excitation (b) Simulated earthquake motion excitation

Figure 10: Maximum angular acceleration at the slab center.

First, we consider the possibility that the torsional response was excited by *Q–Δ* resonance conditions other than $f_{1x} + f_{1y} = f_{2\theta}$ and $f_{2x} - f_{1y} = f_{2\theta}$. In order to confirm which torsional mode was excited, a third-order Butterworth bandpass filter was used to extract the responses close to the first, second, third, and fourth natural frequencies in the torsional direction with passbands of 2.5–2.9 Hz, 6.5–7.3 Hz, 9.8–10.8 Hz, and 14–16 Hz, respectively. **Figure 11** shows the results and the torsional responses of the 2nd to 4th modes are particularly large, with a peak around the resonance condition $f_{2x} - f_{1y} = f_{2\theta} = 6.96$ Hz. For the torsional response where third and fourth modes were excited, there could be *Q–Δ* resonance conditions for higher-order modes other than the 16 *Q–Δ* resonance conditions that consider the first and second modes.

Other possible factors include a minor eccentricity in the small-scale specimen due to manufacturing imperfection and the coupling of the translational and torsional modes.

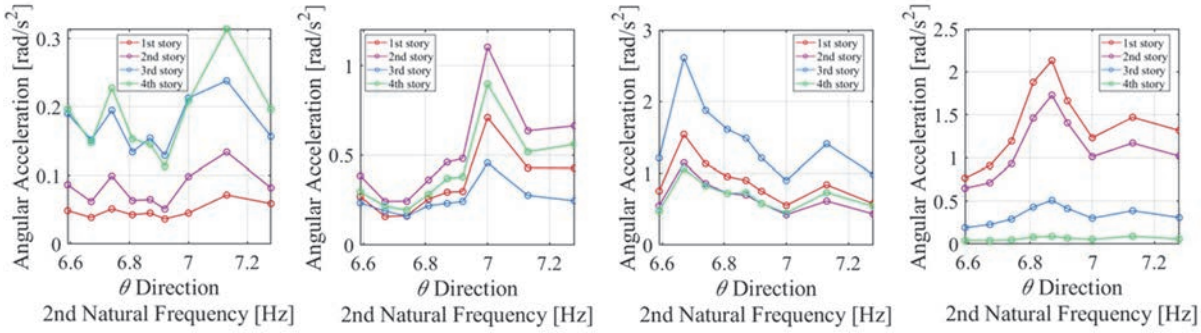

(a) 1st mode (b) 2nd mode (c) 3rd mode (d) 4th mode

Figure 11: Maximum angular acceleration of the slab center after bandpass filtering (Simulated seismic motion excitation).

4 FINITE ELEMENT ANALYSIS TO REPRODUCE THE EXPERIMENT

A finite element model was developed and analyzed to reproduce the shaking table tests of the small-scale specimen. The model is shown in **Fig. 12(a)** and **12(b)**; the numbers of nodes and elements are 22492 and 3136, respectively. The approximately 0.3 m columns were divided into 15 sections by Timoshenko beam elements.

The maximum angular acceleration in experimental and simulation results at P10 under the simulated earthquake motion excitation is shown in **Fig. 13**. The figure shows that the maximum angular acceleration in the simulation is smaller than that in the experiment possibly owing to the damping difference. However, it can be confirmed that the magnitude relationship of the angular acceleration is generally reproduced and the result validates the induction of the torsional response owing to *Q–Δ* resonance.

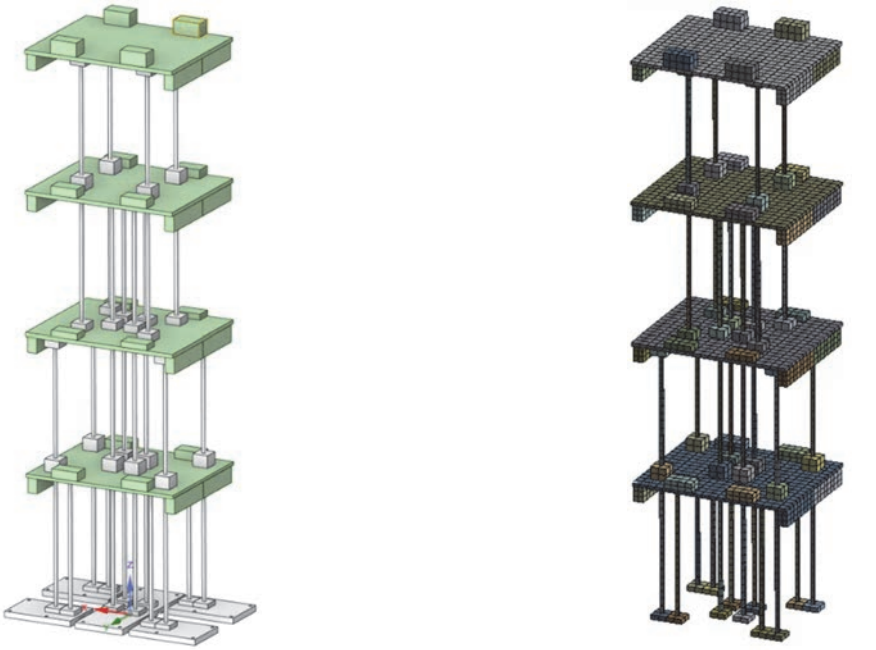

(a) CAD model (b) Finite element model mesh

Figure 12: Finite element model of small-scale specimen.

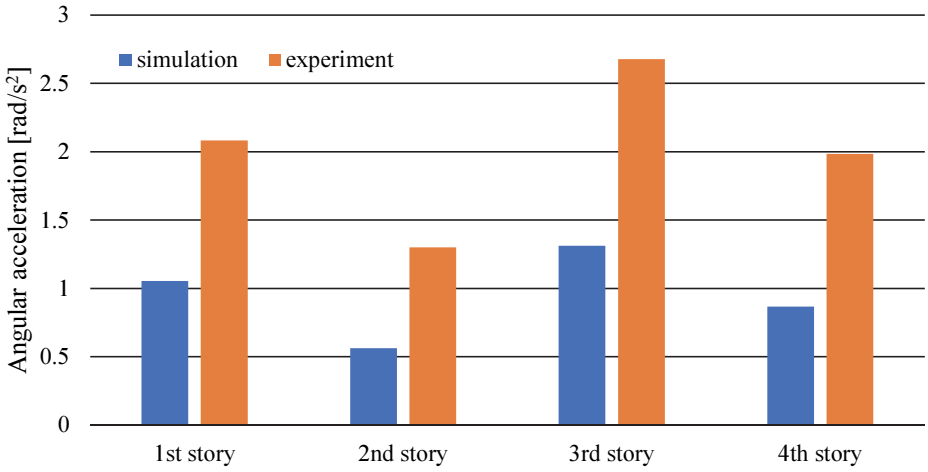

Figure 13: The maximum angular acceleration in experimental and simulated results at P10 under the simulated earthquake motion excitation.

5 CONCLUSIONS

To analyze the characteristics of *Q–Δ* resonance for buildings with a large height/width aspect ratio, where bending deformation is dominant, a small-scale specimen was designed and fabricated, and shaking table experiments were conducted. Sinusoidal waves and simulated earthquake motion were used as input earthquake motion. When sinusoidal waves were input to the specimen, we confirmed that the closer to the *Q–Δ* resonance condition, the more the torsional response was induced. When the simulated earthquake motion was input, it was observed that the third and fourth torsional modes were excited in addition to the second torsional mode. Possible causes include the influence of *Q–Δ* resonance conditions for higher-order modes other than the 16 *Q–Δ* resonance conditions up to the second modes, and the possibility that the torsional response increased due to the coupling of modes in the translational and torsional directions. Finite element analysis was conducted to reproduce the experiment. Although the maximum angular acceleration in the simulation was smaller than that in the experiment possibly owing to the damping difference, the magnitude relationship of the angular acceleration was generally reproduced and the result validates the induction of the torsional response owing to *Q–Δ* resonance.

Future work includes theoretical consideration of the *Q–Δ* resonance condition of higher-order modes and clarification of its effect, and development of a simplified analytical model to study the torsional response.

ACKNOWLEDGMENT

This research was financially supported by SECOM Science and Technology Foundation and JSPS Grant-in-Aid for Scientific Research (B) No. 20H02301.

REFERENCES

[1] Osaka Prefectural Government, General Affairs Department, *Verification Results on the Safety of Osaka Prefectural Government Sakishima Building (May 2011)*, https://www.pref.osaka.lg.jp/otemaemachi/saseibi/bousaitai.html, accessed on March 15, 2023. (in Japanese, title translated by the authors)

[2] M. Kohiyama, H. Yokoyama, Torsional response induced by lateral displacement and inertial force. *Frontiers in Built Environment*, **4**, Article 38, 2018.

[3] F. Mizutori and M. Kohiyama, Experiment of torsional response induced by the Q–Delta resonance. *The Structural Design of Tall and Special Buildings*, **30**, e1829, 2021.

[4] R. Anamizu, M. Kohiyama, Fundamental study of Q–Δ resonance considering higher-order modes by shaking table experiments and finite element analysis. *Journal of Structural Engineering*, Architectural Institute of Japan, **68B**, 386–396, 2022. (in Japanese)

[5] R. Anamizu, Study on simplified model of high-rise building for evaluating Q–Δ resonance using shaking table test and finite element analysis. *Master Thesis of School of Science for Open and Environmental Systems, Graduate School of Science and Technology, Keio University*, 2022. (in Japanese)

[6] Architectural Institute of Japan, *Database of Actual Vibration Measurements of Various Buildings and Structures (December 2020)*, http://news-sv.aij.or.jp/kouzou/s7/d1, accessed on March 15, 2023. (in Japanese, title translated by the authors)

[7] H. R. Tabatabaiefar and B. Mansoury, Detail design, building and commissioning of tall building structural models for experimental shaking table tests. *The Structural Design of Tall and Special Buildings*, **25**, 357–374, 2016.

[8] T. Katayama, *System Identification: Approach from Subspace Method, New Edition*, Asakura Publishing, 109–113, 267, 268, 2018. (in Japanese)

[9] T. Hida and M. Nagano, Estimation Accuracy of Natural Frequency and Damping Factor of Building by System Identification Based on Three Subspace Methods. *Journal of Structural and Construction Engineering*, **79**, 923–932, 2014. (in Japanese)